






## Effect of barnacle fouling on ship resistance and powering

Yigit Kemal Demirel<sup>a</sup> , Dogancan Uzun<sup>a</sup> , Yansheng Zhang<sup>a</sup> , Ho-Chun Fang<sup>b</sup>, Alexander H. Day<sup>a</sup>  and Osman Turan<sup>a</sup> 

<sup>a</sup>Department of Naval Architecture, Ocean and Marine Engineering, University of Strathclyde, Glasgow, UK; <sup>b</sup>Lloyd's Register Global Technology Centre, Lloyd's Register, Southampton, UK

### ABSTRACT

Predictions of added resistance and the effective power of ships were made for varying barnacle fouling conditions. A series of towing tests was carried out using flat plates covered with artificial barnacles. The tests were designed to allow the examination of the effects of barnacle height and percentage coverage on the resistance and effective power of ships. The drag coefficients and roughness function values were evaluated for the flat plates. The roughness effects of the fouling conditions on the ships' frictional resistances were predicted. Added resistance diagrams were then plotted using these predictions, and powering penalties for these ships were calculated using the diagrams generated. The results indicate that the effect of barnacle size is significant, since a 10% coverage of barnacles each 5 mm in height caused a similar level of added power requirements to a 50% coverage of barnacles each 1.25 mm in height.

### ARTICLE HISTORY

Received 19 May 2017  
Accepted 22 August 2017

### KEYWORDS

Artificial barnacles;  
experiment; added  
resistance; powering;  
biofouling


### Introduction

The roughness of a ship's hull, which is often caused by failure of marine coatings and biofouling, can substantially increase frictional resistance and hence fuel consumption and greenhouse gas emissions. Although a large body of research has been devoted to assess the effects of fouling on ship resistance and powering, little effort has been made to classify fouling conditions and relate them to full-scale ship frictional resistance.

Experimental and laboratory-scale studies provide reliable data since the uncertainties can be estimated accurately. Therefore, several experimental studies have been devoted to investigating the roughness effect on skin friction. The first experimental investigation into the effect of hull roughness on frictional resistance can be attributed to Froude (1872, 1874). McEntee (1915) conducted the first extensive experimental study investigating the effect of fouling on frictional resistance (Woods Hole Oceanographic 1952). Flat plates were coated with anticorrosive paints and kept in water for a given period of time, before being towed with barnacles on them. The findings revealed that the resistance of the plates after sea exposure for 12 months increased by four times compared with the resistance of an otherwise identical clean plate (McEntee 1915). Kempf (1937) conducted tests on

pontoons covered with shell fouling and made predictions of the added resistance based on barnacle height and coverage. He recorded a maximum resistance increase when barnacle coverage was 75%. On the other hand, 66% of the maximum drag increase was observed when barnacle coverage was only 5%. The increase in the frictional resistances of surfaces covered with slime was surveyed by Benson et al. (1938) who conducted towing tests of flat plates, as well as performing experiments on cylinders and rotating discs; in addition Watanabe et al. (1969) used a model ship. Lewkowicz and Das (1986) conducted towing tests of flat plates covered with artificial slime, and the increase in frictional resistance due to the slime was found to be 18% (Schultz and Swain 2000). Loeb et al. (1984) conducted rotating disc experiments using discs covered with several different types of microbial slimes. It was observed that microbial slime led to an increase of 10–20% in frictional resistance. Schultz and Swain (1999) and Schultz (2000) investigated the effects of biofilms and algae on the skin friction coefficients of flat plates using boundary layer measurements. Schultz (2004) carried out towing tests using flat plates exposed to seawater and claimed that the most dominant effect on resistance was the height of the largest barnacles on the plates. Swain et al. (2007) surveyed fouling growth on different

**CONTACT** Yigit Kemal Demirel  yigit.demirel@strath.ac.uk

 The supplemental material for this paper is available online at <http://doi.org/10.1080/08927014.2017.1373279>

© 2017 The Author(s). Published by Informa UK Limited, trading as Taylor & Francis Group.  
This is an Open Access article distributed under the terms of the Creative Commons Attribution License (<http://creativecommons.org/licenses/by/4.0/>), which permits unrestricted use, distribution, and reproduction in any medium, provided the original work is properly cited.

types of coatings under static and dynamic conditions. Andrewartha et al. (2010) measured an increase of 99% in the drag coefficients of test plates due to biofilms in a recirculating water tunnel. Monty et al. (2016) carried out experimental and numerical studies and predicted a 34% increase in total resistance of a very large crude oil carrier due to light calcareous tubeworm fouling. These findings clearly demonstrate the importance of effective antifouling coatings in maintaining ship efficiency in operational conditions. Although these experimental studies presented reliable information on a range of fouling types, none of them present a well-defined parametric study in order to provide detailed insight into the effect of barnacle height and coverage on the frictional resistance of a ship. Thus, the aim of this study was to fill this gap by carrying out a systematic experimental and numerical study to assess the effect of barnacle height and coverage on ship resistance and powering.

With the aim of developing a scientific and fundamentally sound approach for predicting the effect of biofouling on added resistance, and hence the increase in power requirements, this paper presents a novel experimental approach (ie using 3-D printed artificial barnacles in order to systematically determine the effects of different levels of fouling growth and coverage on the hydrodynamic resistance of plates) towards establishing a method to predict the added resistance caused by calcareous fouling.

A well-known similarity law scaling procedure from Granville (1958) can be used to predict the effect of such roughness on the frictional resistance of flat plates of ship lengths, provided that the roughness function behaviour of such fouling is known (Schultz 2007). Some examples of the use of this method are given by Flack and Schultz (2010), Schultz et al. (2011), Demirel et al. (2013), Turan et al. (2016), and Kiosidou et al. (2017). Walker et al. (2014) conducted experiments using both antifouling and fouling-release hull coatings and scaled up the results to predict the effects of these coatings on a mid-sized naval ship. Schultz (2007) proposed a methodology to predict the effects of a range of coating and biofouling conditions on ship frictional resistance, using his experimental data, by means of the similarity law scaling procedure of Granville (1958). However, it may be difficult for less experienced users to carry out such an analysis using this methodology. Simple added resistance diagrams for predicting the effect of biofouling on ship frictional resistance would therefore be of great benefit. One of the aims of the present paper was subsequently to generate such diagrams using an in-house code based on the similarity law scaling procedure of Granville (1958), for a given set of fouling conditions.

The proposed diagrams enabled the prediction of the added frictional resistance coefficients of the ships in

question, due to the given fouling coverage on their hulls for a range of ship speeds.

## Experimental facilities, model details and method

The experiments were carried out at the Kelvin Hydrodynamics Laboratory (KHL) of the University of Strathclyde. The KHL test tank has dimensions of 76.0 m × 4.6 m × 2.5 m. The tank is equipped with a digitally controlled towing carriage, a state-of-the-art absorbing wave maker, and a highly effective sloping beach. The carriage has a velocity range of 0–5 m s<sup>-1</sup>, with the velocity range used in these experiments kept between 1.5 and 3.6 m s<sup>-1</sup>. Fresh water was used in the experiments, wherein the temperature of the water was monitored in order to be able to evaluate drag coefficients according to the temperature.

The flat plates used for the tests were manufactured from 304 stainless steel grade sheet stock. Figure 1 depicts the dimensions of the flat plates. The leading edges of the plates were shaped to a radius of 2.5 mm while the trailing edge was kept sharp in order to mitigate the extra drag due to flow separation as much as possible. The flatness of the plates, as well as their dimensions, were checked using a CNC machine.

Actual barnacles of differing sizes, which represent time-based variations in fouling, were scanned in 3-D in order to generate a CAD model of typical barnacle geometries. *Balanus improvisus*, an adult juvenile barnacle species which can grow up to 10 mm in diameter and 5 mm in height (big sized barnacle model) was selected to represent calcareous type fouling (Newman and Abbott 1980). In order to simulate the effects of growing stages of barnacles, middle sized and small sized barnacle models were derived through 3-D scaling from the big sized barnacle model, based on observations from ships' hulls, as well as the studies of Larsson et al. (2010) and Schultz (2004). The derived dimensions were 5 mm in diameter and 2.5 mm in height for a middle sized barnacle, and 2.5 mm in diameter and 1.25 mm in height for a small sized barnacle. The digital models of the barnacles were then printed in 3-D using 3-D printing technology to generate artificial barnacles. Figure S1 in Supplemental material shows a sample of the digital model of the 3-D printed barnacle tiles (50 mm × 50 mm).

The artificial barnacles were glued onto the surfaces of the flat plates and then towing tests of the flat plates were conducted at a range of speeds. In these tests, the plates were installed on a custom-built test rig on the towing carriage and carefully aligned with the centreline of the tank in order to minimise side forces, as seen in Figures 2 and 3. The plates were then towed down the tank using the

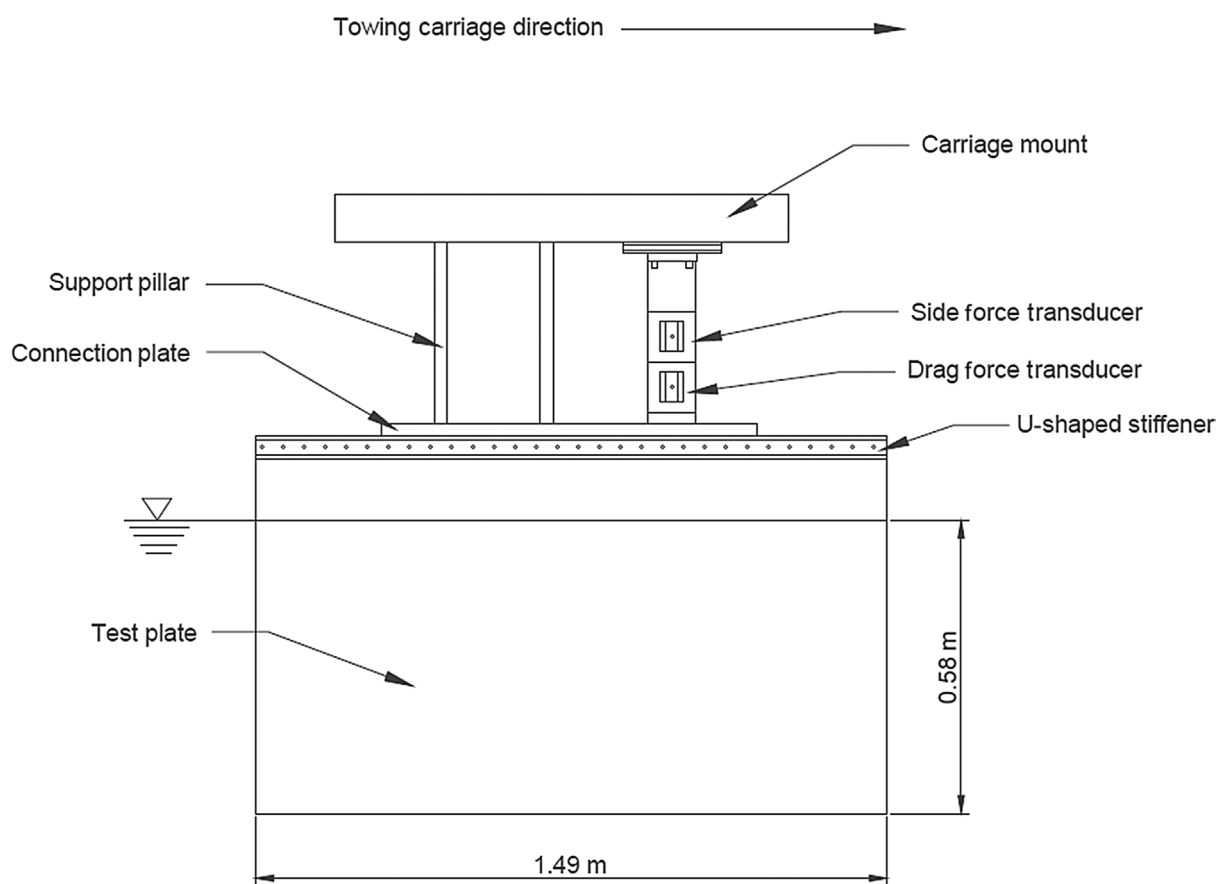


Figure 1. Schematic of the flat plate test fixture.

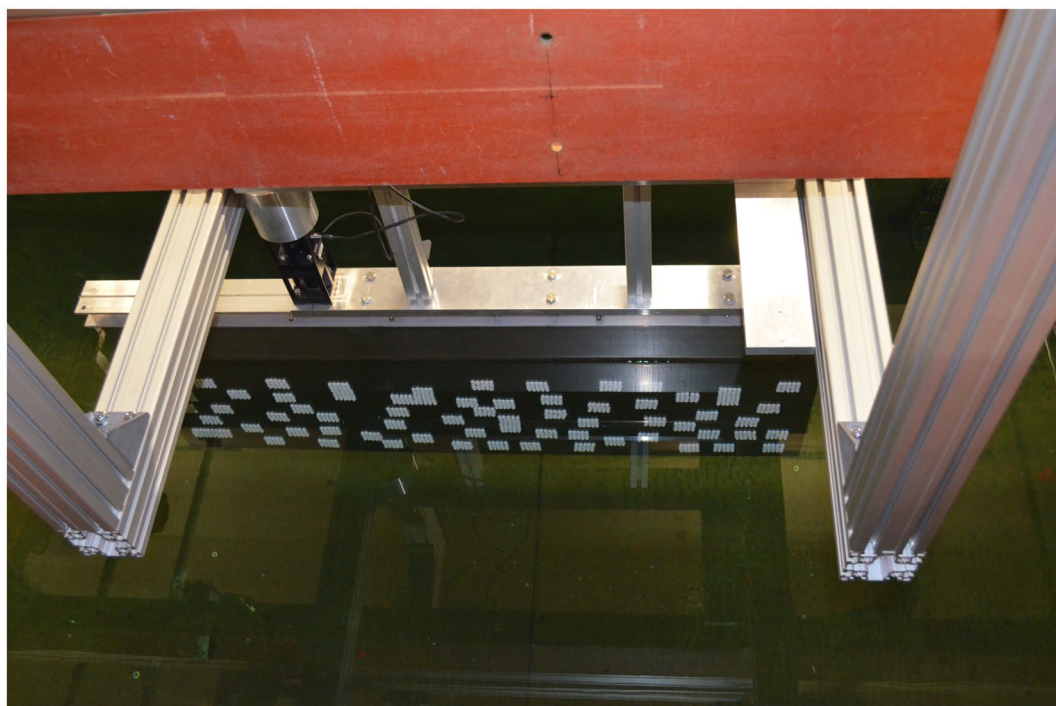


Figure 2. The plate in the tank.





**Figure 3.** Test set-up.

towing carriage at a range of speeds of  $1.5\text{--}3.6\text{ m s}^{-1}$ . The towing force was measured using a load cell, and the side-force was monitored in order to ensure that the plates were correctly aligned in the tank. The carriage speed was accurately measured using a digital encoder on a calibrated wheel. Figure 3 demonstrates the test set-up.

The roughness functions and roughness Reynolds number were then evaluated using the overall drag method of Granville (1987) using the present experimental data. The experimental uncertainty of the results obtained is discussed later.

This technique provides a unique opportunity to systematically determine the effects of different levels of fouling growth and coverage on the hydrodynamic resistance of plates. This systematic approach also eliminates the problems and uncertainties which are encountered during the transportation of the immersed plates from the sea to the tank, including the transfer of the marine life from seawater to freshwater.

Four different coverage percentages and barnacle dimensions, with even distributions and three bare plates, which serve as reference plates, are considered in the experiments. The configurations are shown in Table 1.

The reference plate was the plate onto which the artificial barnacles were glued. Therefore, firstly the reference plate was towed in the tank when it was bare, in order

**Table 1.** Configuration table showing coverages, dimensions and the tests conducted.

Barnacle type	Dimensions (diameter and height)	Reference plate	10% Coverage	20% Coverage	40% Coverage	50% Coverage
B	10 mm and 5 mm	x	x	x		
M	5 mm and 2.5 mm	x	x	x	x	x
S	2.5 mm and 1.25 mm	x	x	x	x	x

to obtain the drag baseline for the other configurations. Following the completion of the tests for this initially bare reference plate, the plate was removed from the water and B-type barnacles were glued on to achieve 10% coverage. The plate was then put back into the water and the same procedure was repeated for 20% surface coverage. After completing B-type barnacle tests, the same procedural sequence was implemented for M-type and S-type barnacle experimental configurations, but with 40 and 50% coverage percentages. The repeatability tests were performed for each surface condition at two different speeds, namely  $1.857$  and  $3.591\text{ m s}^{-1}$ , which correspond to Reynolds numbers of  $\sim 2.6 \times 10^6$  and  $\sim 5 \times 10^6$ , respectively. The distribution pattern applied to the reference plate followed the recommendations of ASTM-D6990-05 (2011).



**Figure 4.** (a) Reference plate; (b) 10% coverage; (c) 20% coverage; (d) 40% coverage; (e) 50% coverage.

Both sides of plates were covered symmetrically in order to mitigate side forces as much as possible. Figure 4 shows different coverage percentages for S-type barnacles.

The total resistance (drag) of a flat plate,  $R_T$ , is mainly composed of two components, the residuary resistance,  $R_R$ , and the frictional resistance,  $R_F$ , as given by Equation 1:

$$R_T = R_R + R_F \quad (1)$$

Once the total drag,  $R_T$ , values were obtained for each plate and related speeds, they were non-dimensionalised by dividing each term by the dynamic pressure and wetted surface area of the plates. The total drag coefficient,  $C_T$ , was therefore evaluated using the following Equation 2:

$$R_T = \frac{1}{2} \rho S C_T V^2 \quad (2)$$

where  $\rho$  is the density of water,  $S$  is the wetted surface area,  $C_T$  is the total resistance coefficient and  $V$  is the speed.

Showing similarity to the resistance decomposition, the total resistance coefficient,  $C_T$ , is made up of the residuary resistance coefficient,  $C_R$ , and the frictional resistance coefficient,  $C_F$ . Given that the residuary resistance coefficient is a function of the Froude number,  $Fr$ , and the frictional resistance coefficient is a function of the Reynolds number,  $Re$ , the total resistance coefficient can therefore be written in the following form (Schultz 2007):

$$C_T = C_R(Fr) + C_F(Re) \quad (3)$$



The Karman–Schoenherr friction line (Schoenherr 1932) given by Equation 4 for a smooth plate can be used to predict the frictional resistance coefficients of a smooth flat plate. The  $C_F$  values of the reference smooth plate are therefore assumed to be equal to the  $C_F$  values obtained using Equation 4. It is of note that Candries (2001) and Schultz (2004) also showed that Equation 4 can be used for the prediction of the frictional resistance of flat plates:

$$\frac{0.242}{\sqrt{C_F}} = \log(Re.C_F) \quad (4)$$

The differences between the  $C_T$  values obtained using the experimental data and the  $C_F$  values obtained using Equation 4 were assumed to be the  $C_R$  values of the reference plate as shown by Equation 5. The computed  $C_R$  values were taken to be the  $C_R$  values of all the test surfaces (Equation 6), since the residuary resistances of the plates were not expected to be significantly affected by the surface roughness (Schultz 2007). Hence, the  $C_F$  values of the test surfaces were computed by subtracting the  $C_R$  values of the reference plate from the  $C_T$  values of the test surfaces as shown by Equation 7. The mathematical process for this is outlined below:

$$C_{R_s} = C_{T_s} - C_{F_s} \quad (5)$$

$$C_{R_s} = C_{R_r} \quad (6)$$

$$C_{F_r} = C_{T_r} - C_{R_r} \quad (7)$$

where the subscript S indicates a smooth condition, whereas the subscript R indicates a rough condition. It should be noted that, within this study, the drag of barnacles is assumed to qualify purely as skin friction drag, since the pressure drag is expected to be insignificant when compared to the frictional drag of the barnacles. This assumption is in accordance with the literature (eg Schultz 2004) and it enables the investigator to use the overall drag method procedure of Granville (1987) and the similarity law scaling procedure of Granville (1958). Roughness Reynolds numbers,  $k^+$ , and roughness function values,  $\Delta U^+$ , for all of the surfaces were obtained iteratively using Equations 8 and 9 following the overall drag method procedure of Granville (1987) using the present experimental data.

$$k^+ = \left(\frac{k}{L}\right) \left(\frac{Re C_F}{2}\right) \left(\sqrt{\frac{2}{C_F}}\right)_R \left[1 - \frac{1}{\kappa} \left(\sqrt{\frac{C_F}{2}}\right)_R + \frac{1}{\kappa} \left(\frac{3}{2\kappa} - \Delta U^+\right) \left(\frac{C_F}{2}\right)_R\right] \quad (8)$$

$$\Delta U^+ = \left(\sqrt{\frac{2}{C_F}}\right)_S - \left(\sqrt{\frac{2}{C_F}}\right)_R - 19.7 \left[ \left(\sqrt{\frac{C_F}{2}}\right)_S - \left(\sqrt{\frac{C_F}{2}}\right)_R \right] - \frac{1}{\kappa} \Delta U^+ \left(\sqrt{\frac{C_F}{2}}\right)_R \quad (9)$$

where L is the plate length, Re is the Reynolds number,  $C_F$  is the frictional drag coefficient, and  $\Delta U^+$  is the roughness function slope, which is the slope of  $\Delta U^+$  as a function of  $\ln(k^+)$ . The subscript S indicates a smooth condition whereas the subscript R indicates a rough condition, and the superscript + indicates the inner variables normalised with  $U_\tau$  or  $U_\tau/\nu$  ( $U_\tau$  is the friction velocity and  $\nu$  is the kinematic viscosity of the fluid).

The prediction code was developed based on the similarity law scaling procedure of Granville (1958), which is explained in detail in Schultz (1998, 2007). The evaluated  $k^+$  and  $\Delta U^+$  values were then employed in the aforementioned code and predictions were made of the roughness effects of these particular fouling conditions on the frictional resistance of flat plates of different lengths representing different ships. Full details of the procedure can be found in Demirel (2015).

In order to reveal the effect of biofouling on fuel consumption, the increase in the total resistance and hence the effective power of the ships in question were calculated. An increase in the total resistance would increase the effective power,  $P_E$ , of a ship, which is the necessary power to move a ship through water.  $P_E$  is related to the total resistance,  $R_T$ , and ship speed,  $V$ , which is defined by Equation 10:

$$P_E = R_T V \quad (10)$$

Equation 2 can then be rewritten for ships as:

$$P_E = \frac{1}{2} \rho S C_T V^3 \quad (11)$$

The increase in the effective power of a ship,  $P_E$ , due to the effect of fouling can be expressed by:

$$\% \Delta P_E = \frac{C_{T_r} - C_{T_s}}{C_{T_s}} \times 100 = \frac{\Delta C_F}{C_{T_s}} \times 100 \quad (12)$$

similar to that used by Tezdogan et al. (2015) and Demirel et al. (2017).  $\Delta C_F$  is the added resistance coefficient due to surface roughness.  $C_{T_s}$ , on the other hand, includes other resistance components and the evaluation of this is not the subject of this study. The  $C_{T_s}$  values of the ships in question were taken from the reports of the experiments that were performed earlier at the Kelvin Hydrodynamics

Laboratory at the University of Strathclyde. It should be noted that all parameters used in Equations 10–12 are parameters belonging to the ships in question.

## Results

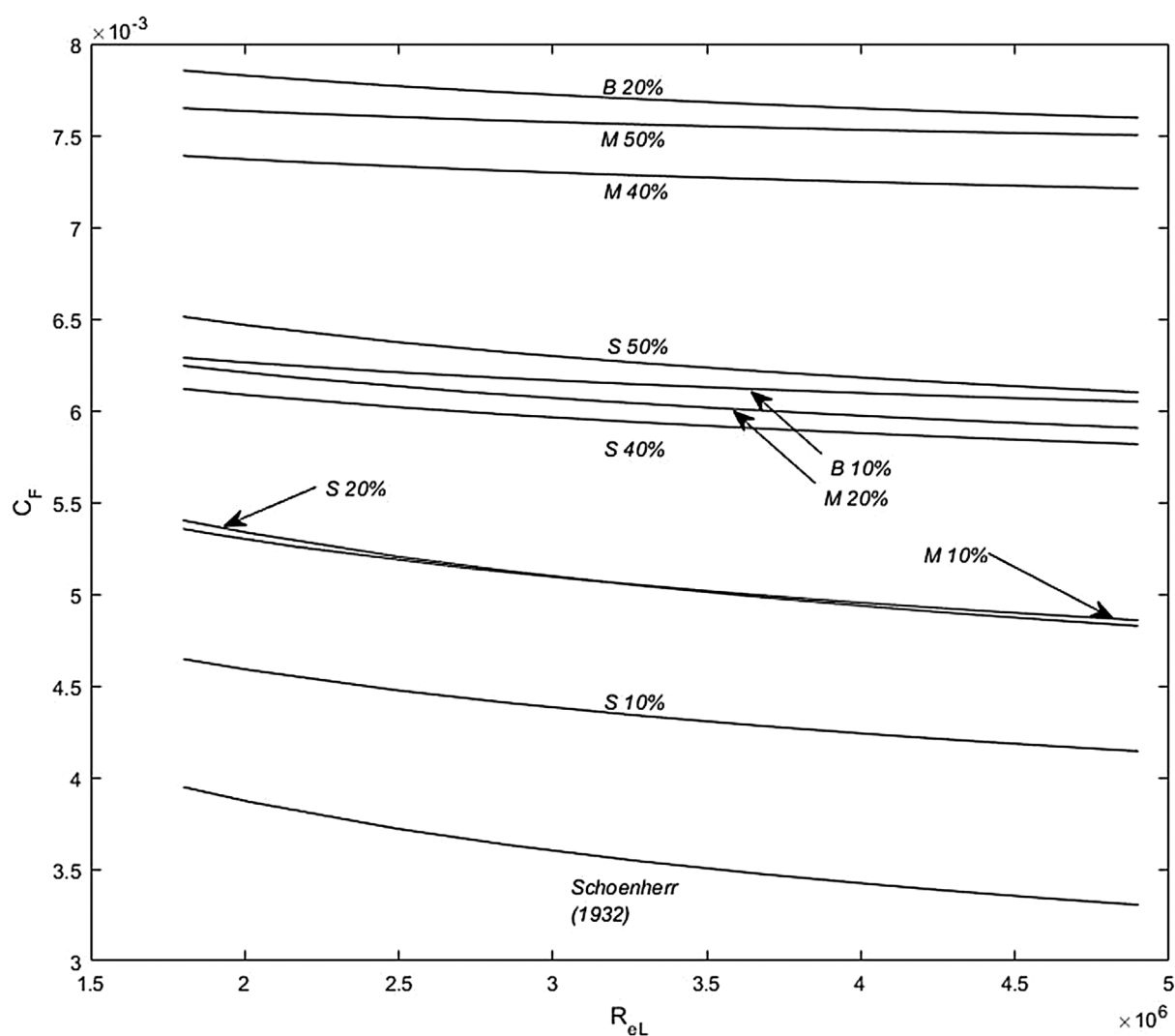
### Frictional resistance

Figure 5 illustrates the frictional resistance coefficients of all the test surfaces. It is clearly seen that B 20% caused the most marked effect on the frictional resistance, with an average increase of 119% with respect to the reference plate. M 50% caused the second largest increase in the frictional resistance (on average 115%), followed by M 40% (on average 107% increase), S 50% (on average 77% increase), B 10% (on average 74% increase), M 20% (on average 71% increase), S 40% (on average 68% increase), M 10% (on average 44% increase), S 20% (on average 43% increase) and S 10% (on average 23% increase).

As can be seen from Figure 5, the size as well as the coverage area by barnacles has effects on the frictional resistance values. In normal circumstances, a friction curve, when flow reaches the fully rough regime, is expected to be independent of Reynolds number. However, all the friction curves in the present study show dependency on Reynolds number even for the severe fouling conditions. This point may need to be further investigated in future studies.

Having conducted experiments using different sized barnacles and different coverage areas, it would be interesting to also investigate the effects of size and area separately. Therefore, the following discussion aims to compare and discuss the results from two different points of view.

The effect of the coverage area on the frictional resistance is highlighted by Figures S2 and S3, which show the frictional resistance coefficients of M-type and S-type surfaces separately; the changes in the  $C_F$  values of the test



**Figure 5.** Frictional resistance coefficients of all the test surfaces. B-type: biggest barnacles; M-type: middle barnacles; S-type: smallest barnacles, and the numbers with percentages represent the coverage of plates.

plates with respect to the reference plate are tabulated in Table 2.

As expected and seen from Figures S2 and S3 and Table 2, the configurations which have higher coverage area have higher  $C_F$  values. The average increases in the  $C_F$  values of the test surfaces due to the presence of M-type barnacles were observed to be 44% for 10%, 71% for 20%, 107% for 40% and 115% for 50%, whereas these values altered to 23% for 10%, 43% for 20%, 68% for 40% and 77% for 50% for surfaces covered with S-type barnacles. It is interesting to note that for lower coverage areas the rates of increase in  $C_F$  values are much higher than the rate for higher coverage areas. For both M-type and S-type surfaces, the  $C_F$  values obtained almost reached a plateau at 40% coverage and the change in  $C_F$  values beyond 40% was comparatively smaller at 50% coverage. The authors believe the outcome suggests that after a certain threshold, an increase in the coverage area would have minor effect on the frictional resistance. It is important to note that these findings are in accordance with the findings of Kempf (1937), Macdonald (2000) and Schultz (2004). Further study is needed to assess the validity of this assumption.

The effect of barnacle size on the frictional resistance is highlighted by Figures S4 and S5, which show the frictional resistance coefficients for 10 and 20% coverages separately, and the changes in the  $C_F$  values of the test plates with respect to the reference plate are shown in Table 3.

As expected and seen from Figures S4 and S5 and Table 3, the frictional resistance increased with increasing barnacle sizes. The average increase in the  $C_F$  values of the test surfaces due to 10% coverage area was found to be 74% for B-type, 44% for M-type and 23% for S-type surfaces, whereas these values were 119% for B-type, 74% for M-type and 43% for S-type surfaces with 20% coverage. It is important to note that the size of a barnacle has a substantial effect on the frictional resistance and the

**Table 2.** Change in the  $C_F$  values of the test plates with respect to the reference plate.

Configuration	Average change in $C_F$ (%)	Configuration	Average change in $C_F$ (%)
M 10%	44	S 10%	23
M 20%	71	S 20%	43
M 40%	107	S 40%	68
M 50%	115	S 50%	77

**Table 3.** Change in  $C_F$  values of the test plates with respect to the reference plate.

Configuration	Average change in $C_F$ (%)	Configuration	Average change in $C_F$ (%)
B 10%	74	B 20%	119
M 10%	44	M 20%	74
S 10%	23	S 20%	43

results do not show a reduction in the rate of increase in  $C_F$  values, contrary to the results shown in Figures S2 and S3 and Table 2. An interesting point to note is that the effect of a particular hard-shell fouling condition on frictional resistance is more dominant at lower speeds.

### Roughness functions

Shown for comparison in Figure 6 is the Colebrook type roughness function of Grigson (1992), the analytical fit of Ioselevich and Pilipenko (1974) based on the roughness function data of Nikuradse (1933), the analytical fit of Demirel et al. (2017) based on the roughness functions of Schultz and Flack (2007) and the roughness functions of fouled surfaces of Schultz (2004), together with the roughness functions of the present test surfaces, using a logarithmic scale in the x-axis. It should be taken into account that the roughness Reynolds numbers of present test surfaces shown in Figure 6 were calculated using  $k = 0.059h(\%coverage)^{1/2}$  as the roughness length scale, as per the suggestion of Schultz (2004) where  $h$  is the barnacle height.

It is clear from Figure 6 that all the surfaces show a monotonically increasing trend with the increasing roughness Reynolds numbers, which is in agreement with the behaviour of the roughness functions of Grigson (1992). Therefore, the roughness functions of the surfaces can be defined by the roughness function model of Grigson (1992) given that the roughness length scale is chosen accordingly. It is interesting to note that B 10%, M 10% and S 20% collapsed to a so-called group, such that they can be defined by a single roughness function model using the same scaling.

The silicone 1 and silicone 2 surfaces of Schultz (2004) have much larger roughness function values than the present test surfaces since both surfaces have bigger ( $\sim 6$  and  $\sim 7$  mm in height, respectively) barnacles and coverages (60% and 75% coverage, respectively). Although the Self Polishing Copolymer (SPC) copper and ablative copper surfaces of Schultz (2004) have the same barnacle height as B-type surfaces (5 mm in height) in the present study and much lower barnacle percentage coverage (4% and 1% coverage, respectively), both surfaces have higher roughness function values than B 10%. This may be attributed to the existence of slime and hydroid accumulations seen on the SPC copper and ablative copper surfaces of Schultz (2004), which demonstrates that the existence of slime and hydroids may have more influence on drag than expected.

Although Schultz (2004) used the same roughness length scale formula for several surfaces with barnacles and observed an excellent collapse for the results with the Colebrook type roughness function model of Grigson (1992), the present study clearly showed that using one



roughness length scale including barnacle height and coverage for surfaces with barnacles did not lead to a collapse with any given roughness function model and they show a systematic variation. However, by using different scaling for each test surface, excellent collapse with the Colebrook type roughness function model can be achieved since the behaviours of the roughness functions showed a very good agreement with the roughness function model proposed by Grigson (1992). For this reason, rather than trying to correlate measurable surface properties with this roughness function model, for each test surface so-called hydrodynamic roughness length scales,  $k_G$ , that give the same roughness Reynolds numbers with corresponding roughness function values of Grigson (1992), were obtained using reverse engineering. It should be noted that these hydrodynamic roughness length scales,  $k_G$ , are not a function of measurable surface properties and may be termed as experimentally obtained equivalent roughness height. However, using  $k_G$  is very useful for modelling since each  $k_G$  value given in Table 4 represents the corresponding test surface when used together with the roughness function model of Grigson (1992) *via* Equation 13. These hydrodynamic length scales,  $k_G$ , can be used to determine the roughness Reynolds numbers and the roughness function

values of the corresponding surfaces, because the roughness function behaviours of the test surfaces follow the roughness function model of Grigson (1992) given as:

$$\Delta U^+ = \left(\frac{1}{\kappa}\right) \ln(1 + k^+) \quad (13)$$

Figure 7 demonstrates the excellent agreement between the roughness functions of the present test surfaces with the Colebrook type roughness functions of Grigson (1992), when  $k_G$  values are used as the length scale. It should be noted that the roughness Reynolds numbers of the surfaces of Schultz (2004) shown in Figure 7 were calculated using  $k = 0.059 h(\% \text{coverage})^{1/2}$  as the roughness length scale, as per the suggestion of Schultz (2004). Given that  $k_G$  values are experimentally obtained parameters, this suggests that investigators are still obliged to carry out experiments to determine the roughness functions of fouled surfaces. However, once the roughness functions and the roughness function behaviours are determined experimentally, the effect of these very surfaces on the resistances of any arbitrary body can then be predicted using either the similarity law procedure (eg Granville (1958)) or the state-of-the-art computational fluid dynamics (eg Demirel et al. 2014, 2017).

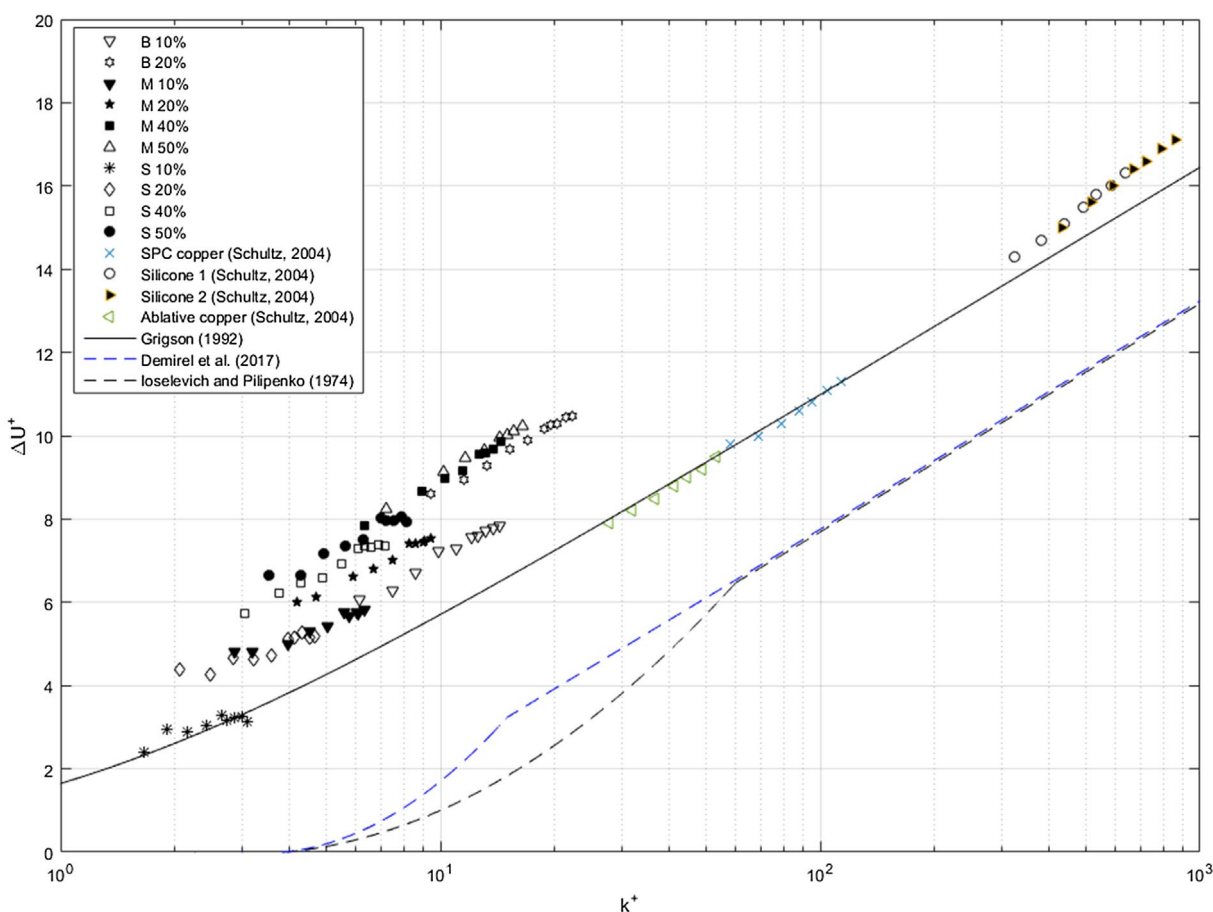


Figure 6. Roughness functions for all the test surfaces ( $k=0.059 h(\% \text{ coverage})^{1/2}$ ) together with roughness function models.

The authors believe that the question of how to correlate the roughness functions of fouled surfaces with the measurable parameters is a question far from being answered. However, an effort has been made to define corresponding  $k_G$  values using the present measurable parameters, ie barnacle height and percentage coverage, in order to practically estimate the effect of any barnacle fouling that falls within the limits of the present barnacle fouled surfaces. Therefore, a third degree polynomial surface was fitted as shown in Figure 8, and based on the

**Table 4.** Experimentally obtained roughness length scales,  $k_G$ , and measurable surface properties of the test surfaces.

Test surface	$k_G$ ( $\mu\text{m}$ )	$k_G$ ( $\mu\text{m}$ ) (Regression)	h (mm)	Surface coverage (%)
B 10%	174	174	5	10
B 20%	489	445	5	20
M 10%	84	93	2.5	10
M 20%	165	172	2.5	20
M 40%	388	390	2.5	40
M 50%	460	443	2.5	50
S 10%	24	22	1.25	10
S 20%	63	64	1.25	20
S 40%	149	166	1.25	40
S 50%	194	183	1.25	50

surface given in Figure 8, the following roughness length scale was developed for the barnacle fouled surfaces.

$$k_G = f(SC, h) = 52 - 5.66(SC) + 28.2h + 0.3(SC)^2 + 1.9435(SC)h - 13.1h^2 - 0.00354(SC)^3 - 0.018(SC)^2h + (SC)h^2 \quad (14)$$

where  $k_G$  is hydrodynamic roughness length scale that gives the same roughness Reynolds numbers with corresponding roughness function values of Grigson (1992), in  $\mu\text{m}$ , SC is percentage coverage and h is barnacle height in mm. Equation 14 may be used to predict the  $k_G$  value of a barnacle-fouled surface that falls within the limits of the present barnacle fouled surfaces and hence this  $k_G$  value may be used to calculate the corresponding roughness Reynolds number,  $k^+$ , and roughness function value,  $\Delta U^+$ , without being obliged to conduct further experiments. However, this equation may not necessarily represent all barnacle fouling conditions due to the fact that it was generated based solely on the results of the present study. Further study is needed to assess the validity of this assumption.

The real  $k_G$  values and those obtained by means of regression using Equation 14 are given in Table 4 for comparison. In spite of the slight discrepancies between

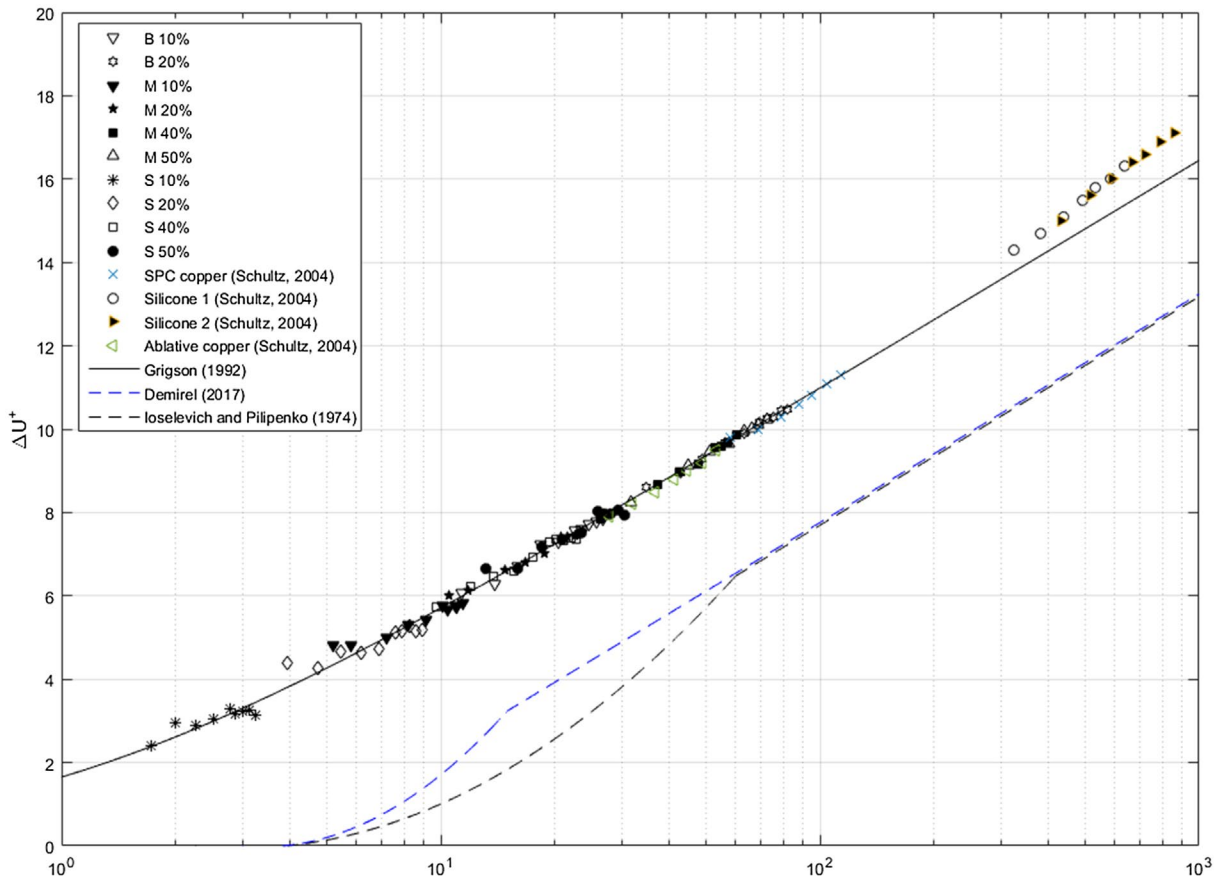


**Figure 7.** Roughness functions for all the present test surfaces, using corresponding  $k_G$  values, together with roughness function models and the surfaces of Schultz (2004).

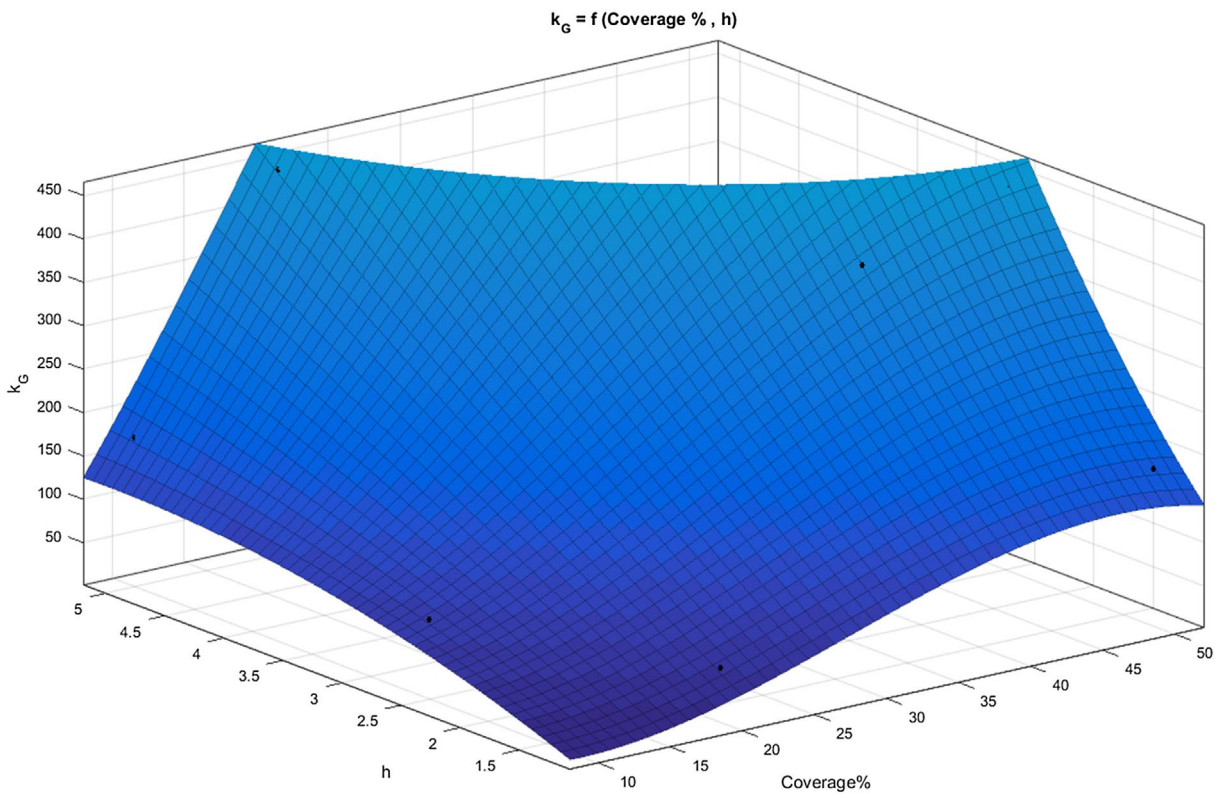


Figure 8. Surface representing  $k_G$  as a function of barnacle height and percentage coverage.

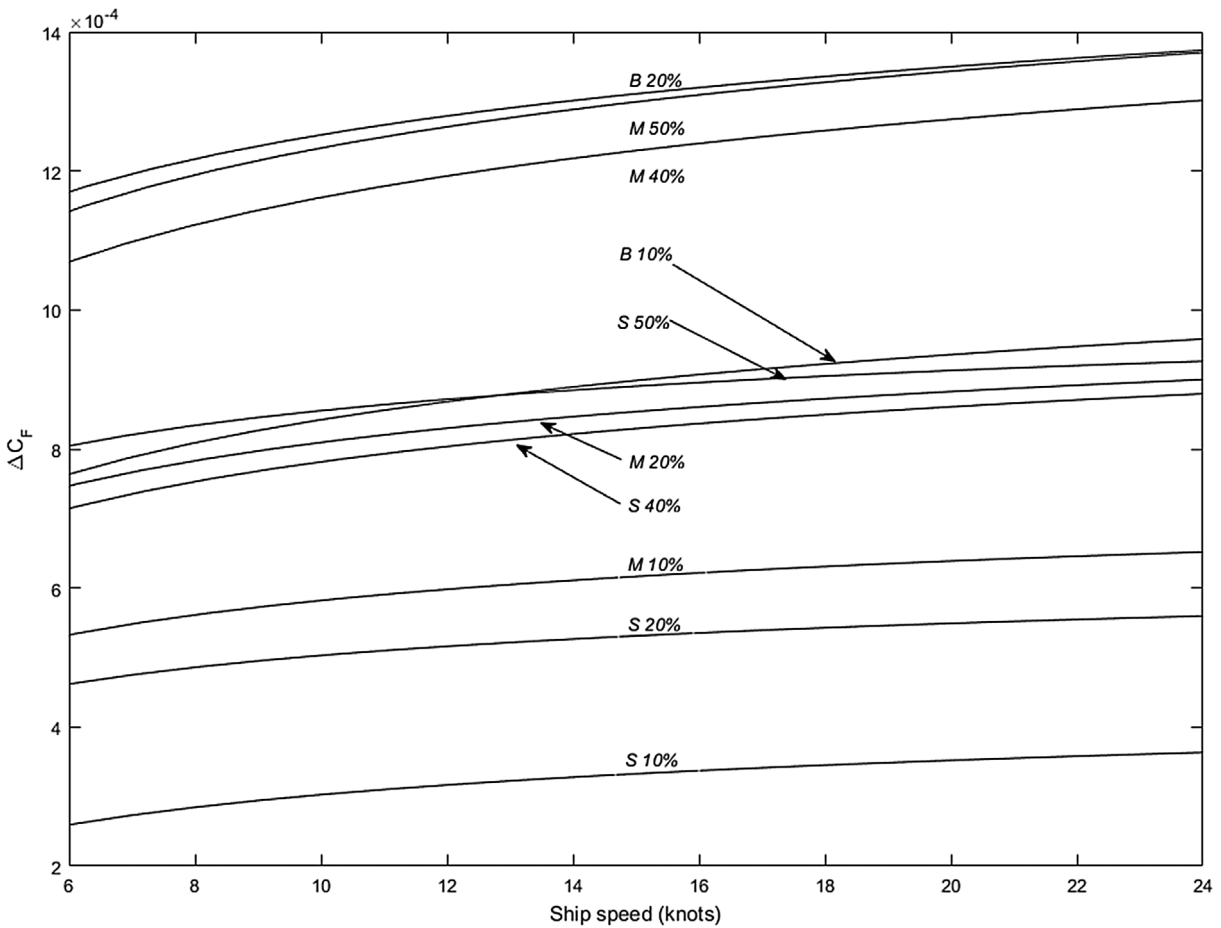
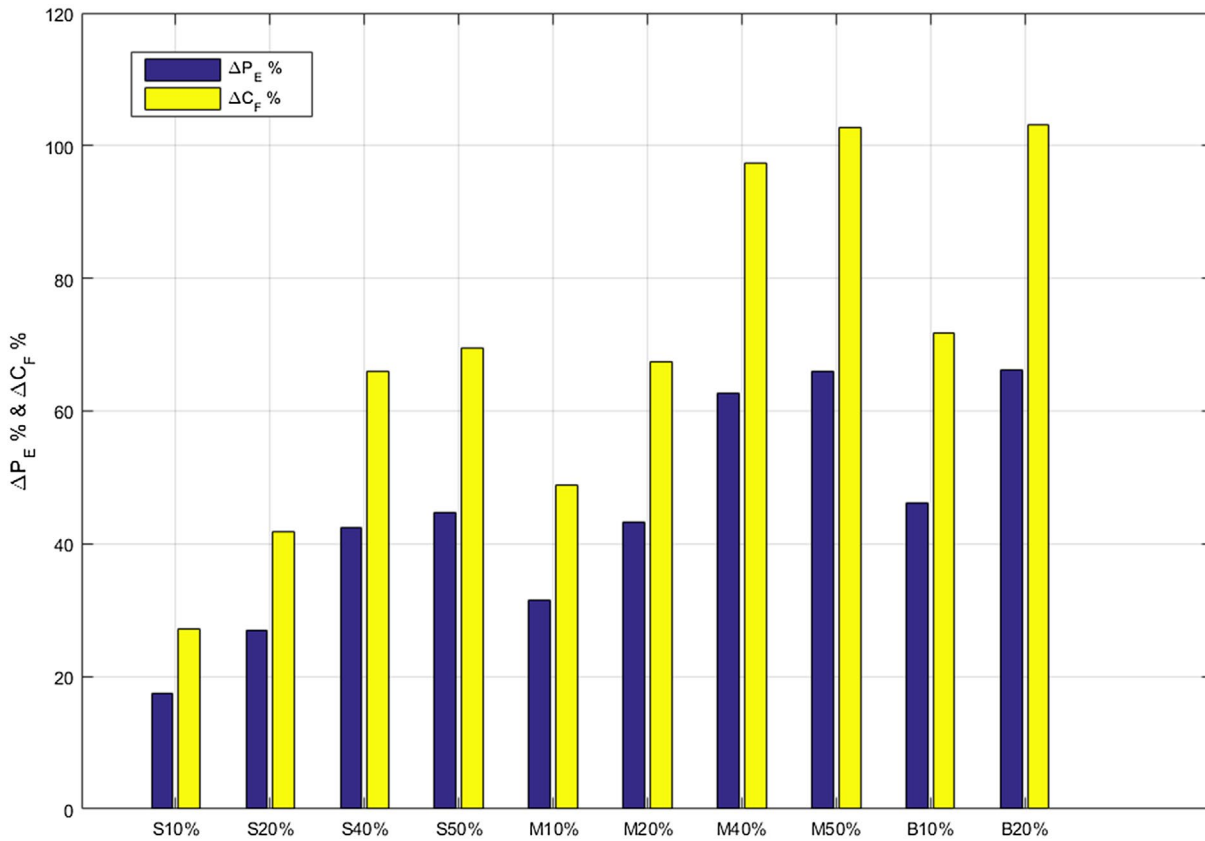


Figure 9. Added resistance diagram for a 230 m container ship with different barnacle fouling conditions.





**Figure 10.** Percentage increases in  $C_F$  and  $P_E$  values of a 230 m container ship with respect to the smooth hull condition.

the individual  $k_G$  values and the  $k_G$  values obtained by regression, good agreement is achieved since these slight discrepancies do not markedly affect the calculated roughness functions.

Ultimately the effect of these very surfaces on the resistances of any arbitrary body can be predicted using either the similarity law procedure (eg Granville 1958) or the state-of-the-art computational fluid dynamics (eg Demirel et al. 2014, 2017). It is clear that Equation 14 may not necessarily represent all barnacle-fouled surfaces, since the assumptions made are based on the observations made in this study only. Future work may be an investigation into the range of applicability of the selected roughness length scale for other barnacle-fouled configurations.

### Uncertainty estimates

Uncertainty estimates for the drag coefficients and roughness function calculations were made through repeatability tests using the procedure defined by the ITTC (2002). The repeatability tests were performed at two speeds, namely  $1.857 \text{ m s}^{-1}$  and  $3.591 \text{ m s}^{-1}$ , which correspond to Reynolds numbers of  $\sim 2.6 \times 10^6$  and  $\sim 5 \times 10^6$ , respectively.

For the B-type barnacle configuration the bias uncertainty in  $C_F$  ranged from  $\pm 1.9\%$  at the lowest Reynolds

number to  $\pm 0.7\%$  at the highest Reynolds number, while the precision uncertainty in  $C_F$  ranged from  $\pm 0.6\%$  at the lower Reynolds number to  $\pm 0.2\%$  at the higher Reynolds number. The overall uncertainty in  $C_F$  ranged from  $\pm 2.0\%$  at the lower Reynolds number to  $\pm 0.7\%$  at the higher Reynolds number. Total uncertainty in  $\Delta U^+$  ranged from  $\pm 5.3\%$  at the lowest Reynolds number to  $\pm 0.8\%$  at highest Reynolds number for this type.

For the M-type barnacle configuration, the result bias and precision uncertainty in  $C_F$  ranged from  $\pm 3.4\%$  at the lowest Reynolds number to  $\pm 1.8\%$  at the highest Reynolds number while in  $\Delta U^+$  uncertainty values remained between  $\pm 5.7\%$  and  $\pm 2.6\%$  respectively in lower and higher Reynolds number.

For the S-type barnacle configuration, bias and precision uncertainty in  $C_F$  ranged from  $\pm 3.4\%$  at the lowest Reynolds number to  $\pm 1.3\%$  at the highest Reynolds number while in  $\Delta U^+$  uncertainty values remained between  $\pm 27.7\%$  and  $\pm 6.7\%$  respectively in lowest and highest Reynolds number.

The overall uncertainty levels of the drag coefficients are satisfactory in comparison to other experiments given in the literature such as Schultz (2004). The very small precision limits reveal the acceptable repeatability of the experiments.

### Effect of added resistance due to calcareous fouling on the effective power of ships

The roughness functions and roughness Reynolds numbers given in the previous section were employed in the prediction code, and predictions of the added resistance coefficients,  $\Delta C_F$ , were made for all fouling conditions. Predictions were made for flat plates representing a container ship of 230 m, a bulk carrier of 180 m, a bulk carrier of 280 m, a cruise ship of 280 m, a tanker of 250 m, a special purpose vessel of 60 m, a special purpose vessel of 120 m and an LNG carrier of 270 m. The added resistance coefficients,  $\Delta C_F$ , due to the given fouling conditions were plotted against several ship speeds. Logarithmic equations were then fitted to the  $\Delta C_F$  values using the least squares method in order to evaluate added resistance diagrams.

Figure 9 shows the added resistance diagram for a 230 m container ship with different fouling conditions whereas Figure 10 demonstrates the increases in the frictional and total resistance and hence in the effective power of the containership at a design speed of 24 knots. The added resistance diagrams and corresponding graphs for other ship types are given in Figures S6–S19.

The increases in the  $C_F$  and  $P_E$  values of the containership due to S-type barnacle accumulation at a ship speed of 24 knots were predicted to be 27% and 17.5% for 10% coverage; 42% and 27% for 20% coverage; 66% and 42% for 40% coverage; and 69.5% and 44.6% for 50% coverage. These values changed to 49% and 31% for 10% coverage; 67% and 43% for 20% coverage; 97% and 63% for 40% coverage; and 103% and 66% for 50% coverage for M-type barnacle accumulation. The increases in  $C_F$  and  $P_E$  were predicted to be 72% and 46% for 10% coverage and 103% and 66% for 20% coverage for B-type surface condition. The effect of size of barnacle on added resistance is significant as 10% coverage of B-type surface causes the same level of added power requirements as 50% coverage of S-type surface.

### Discussion and conclusions

An experimental and numerical study of the effect of barnacle fouling on ship resistance and powering was carried out and the drag characteristics obtained were then scaled to full-scale ship characteristics and the effects of different barnacle fouling conditions on the effective power of ships were predicted.

The plates were towed at a range of speeds and the total resistances of the surfaces were measured. The resistance values were then non-dimensionalised. The frictional resistance coefficients of all of the test surfaces were computed using assumptions that suggest the frictional resistance coefficients of smooth surfaces obey the Karman–Schoenherr

friction line (Schoenherr 1932), and that the residuary resistances of flat plates are not affected by surface roughness. Subsequently, roughness function values of all of the test surfaces were calculated using an indirect method, following the overall drag method of Granville (1987). Uncertainty estimates were made through repeatability tests, with the uncertainty values found to be sufficient to ensure a reliable comparison. Following this, the roughness functions obtained and roughness Reynolds numbers were employed in an in-house code developed based on the similarity law analysis of Granville (1958). The added frictional resistance coefficients of flat plates representing different ships types were then predicted for various ship speeds, and added resistance diagrams were generated using these predictions. The increases in the effective power of the ships were then predicted for ship design speeds using the added resistance diagram.

The increases in the frictional resistance and effective power of a full-scale containership of 230 m, at a design speed of 24 knots, were predicted to be 27% and 17.5% for S 10%; 42% and 27% for S 20%; 66% and 42% for S 40%; and 69.5% and 44.6% for S 50%. These values altered to 49% and 31% for M 10%; 67% and 43% for M 20%; 97% and 63% for M 40%; and 103% and 66% for M 50% conditions. The increases in  $C_F$  and  $P_E$  were predicted to be 72% and 46% for 10% coverage and 103% and 66% for 20% coverage for B-type surface condition.

The proposed diagrams have a key advantage in that they capture the complex hydrodynamic response of fouling in simple curves which can be implemented in a spreadsheet or a tool for life-cycle cost estimation. The main advantage of the diagrams is that they directly enable the use of surface conditions, ship length and ship speed, rather than having to use hydrodynamic parameters. By using such diagrams, the added resistance can be estimated, and hence the fuel penalty, of a ship for a particular fouling condition given in this study. Therefore, it becomes very practical to calculate the effect of a range of fouling conditions on ship resistance and powering.

This approach assumes a homogenous distribution of fouling on the flat plates of ships' hulls, which may not necessarily be the case on real ships' hulls and may introduce uncertainties. As a result, additional results from further immersion tests and experiments considering different types of fouling and their spatial distributions would be beneficial to improve the diagrams. Future studies may include the investigation of the roughness function behaviours of heterogeneous fouling accumulation, as seen on hulls.

This paper also provides the algorithm of a prediction procedure, showing how to develop such diagrams using the available experimental data. Having shown the applicability of the artificial fouling organisms and the

methods used in this study, a future experimental study might be to test different sizes of barnacles and other types of fouling, and then obtain new roughness function models and generate new added resistance diagrams for the tested surfaces.

Future plans are to employ the roughness functions obtained in this study in the wall-function of a CFD software code, and hence investigate the effects of these barnacle fouling conditions on the performances of ships under more complex flow conditions, such as under the effect of a rotating propeller or a dynamic fluid–body interaction using the approaches suggested by Demirel et al. (2017) and Mizzi et al. (2017). Future work would be the numerical investigation of fouling on the vortex-induced vibrations (VIVs) of a floating marine structure. For example, the study of Holland et al. (2017), who performed a series of VIV simulations on a semi-submersible geometry using CFD, could be extended to analyse the effect of fouling on VIVs.

## Nomenclature

$k$	roughness length scale
$k^+$	roughness Reynolds number
$\kappa$	von Karman constant
$\rho$	density
$\nu$	kinematic viscosity
$U_\tau$	friction velocity
$\Delta U^+$	roughness function
$\Delta U^+$	slope of roughness function
$h$	barnacle height
$k_G$	experimentally obtained equivalent roughness length scale
$SC$	surface coverage (%)
B-type	biggest type barnacle
M-type	medium type barnacle
S-type	small type barnacle
$L$	plate length
$S$	wetted surface area
$V$	speed
$Fr$	Froude number
$R_e$	Reynolds number
$R_T$	total resistance
$R_F$	frictional resistance
$R_R$	residuary resistance
$P_E$	effective power
$C_T$	total resistance coefficient
$C_F$	frictional resistance coefficient
$C_R$	residuary resistance coefficient
$C_{T_s}$	total resistance coefficient in smooth condition
$C_{F_s}$	frictional resistance coefficient in smooth condition

$C_R$	residuary resistance coefficient in smooth condition
$C_{T_r}$	total resistance coefficient in rough condition
$C_{F_r}$	frictional resistance coefficient in rough condition
$C_{R_r}$	residuary resistance coefficient in rough condition
$\Delta C_F$	added resistance coefficient due to surface roughness
$\Delta P_E$	increase in effective power due to surface roughness

## Acknowledgements

The authors are grateful for EPSRC support for the project on ‘Shipping in Changing Climates’ which enabled them to carry out the research reported in this paper. The authors also gratefully acknowledge that the research presented in this paper was partially generated as part of the EU funded FP7 project FOUL-X-SPEL (Environmentally Friendly Antifouling Technology to Optimise the Energy Efficiency of Ships, FP7-SST-2011-RTD-1). The authors would like to thank Professor Michael P. Schultz for providing his experimental data. The underlying data in this paper are openly available from the University of Strathclyde data repository at: <https://doi.org/10.15129/bc0b8d10-7719-4c6f-8d60-8427aafcb70>

## Disclosure statement

No potential conflict of interest was reported by the authors.

## Funding

This work was supported by Engineering and Physical Sciences Research Council [grant number EP/K039253/1]; FP7 Transport [project number 285552].

## ORCID

Yigit Kemal Demirel  <http://orcid.org/0000-0001-6739-4911>  
 Dogancan Uzun  <http://orcid.org/0000-0001-7092-2674>  
 Yansheng Zhang  <http://orcid.org/0000-0003-1413-5021>  
 Alexander H. Day  <http://orcid.org/0000-0001-6798-3468>  
 Osman Turan  <http://orcid.org/0000-0003-1877-8462>

## References

- Andrewartha J, Perkins K, Sargison J, Osborn J, Walker G, Henderson A, Hallegraef G. 2010. Drag force and surface roughness measurements on freshwater biofouled surfaces. *Biofouling*. 26:487–496.
- ASTM-D6990-05. 2011. Standard practice for evaluating biofouling resistance and physical performance of marine coating systems.
- Benson J, Ebert J, Beery T. 1938. Investigation in the NACA tank of the effect of immersion in salt water on the resistance



- of plates coated with different shipbottom paints. NACA Memorandum Report C&R C-S19-1(3).
- Candries M. 2001. Drag, boundary-layer and roughness characteristics of marine surfaces coated with antifouling [PhD thesis]. Newcastle: University of Newcastle Upon Tyne.
- Demirel YK. 2015. Modelling the roughness effects of marine coatings and biofouling on ship frictional resistance [PhD thesis]. Glasgow: University of Strathclyde.
- Demirel YK, Khorasanchi M, Turan O, Incecik A. 2013. On the importance of antifouling coatings regarding ship resistance and powering. 3rd International Conference on Technologies, Operations, Logistics and Modelling for Low Carbon Shipping; Sep 9–10; London/UK. Available from: [http://www.lowcarbonshipping.co.uk/index.php?option=com\\_content&view=article&id=29&Itemid=164](http://www.lowcarbonshipping.co.uk/index.php?option=com_content&view=article&id=29&Itemid=164); [http://www.lowcarbonshipping.co.uk/files/ucl\\_admin/LCS%202013/Demirel\\_et\\_al.pdf](http://www.lowcarbonshipping.co.uk/files/ucl_admin/LCS%202013/Demirel_et_al.pdf)
- Demirel YK, Khorasanchi M, Turan O, Incecik A, Schultz MP. 2014. A CFD model for the frictional resistance prediction of antifouling coatings. *Ocean Eng.* 89:21–31.
- Demirel YK, Turan O, Incecik A. 2017. Predicting the effect of biofouling on ship resistance using CFD. *Appl Ocean Res.* 62:100–118.
- Flack KA, Schultz MP. 2010. Review of hydraulic roughness scales in the fully rough regime. *J Fluids Eng.* 132:041203–041203.
- Froude W. 1872. Experiments on the surface-friction experienced by a plane moving through water. British Association for the Advancement of Science. The Collected Papers of William Froude, Institution of Naval Architects, 1955; p. 138–146.
- Froude W. 1874. Report to the lords commissioners of the admiralty on experiments for the determination of the frictional resistance of water on a surface, under various conditions, performed at Chelston cross, under the authority of their lordships. 44th Report by the British Association for the Advancement of Science.
- Granville PS. 1958. The frictional resistance and turbulent boundary layer of rough surfaces. *J Ship Res.* 2:52–74.
- Granville PS. 1987. Three indirect methods for the drag characterization of arbitrarily rough surfaces on flat plates. *J Ship Res.* 31:70–77.
- Grigson C. 1992. Drag losses of new ships caused by hull finish. *J Ship Res.* 36:182–196.
- Holland V, Tezdogan T, Oguz E. 2017. Full-scale CFD investigations of helical strakes as a means of reducing the vortex induced forces on a semi-submersible. *Ocean Eng.* 137:338–351.
- Iosevich VA, Pilipenko VN. 1974. Logarithmic velocity profile for flow of a weak polymer solution near a rough surface. *Soviet Physics Doklady*; p. 18–790 Available from: <http://adsabs.harvard.edu/abs/1974SPhD..18.790I>.
- ITTC. 2002. Uncertainty analysis, example for resistance test. ITTC recommended procedures and guidelines, Procedure 75-02-02-02, Revision 01.
- Kempf G. 1937. On the effect of roughness on the resistance of ships. *Trans INA.* 79:109–119.
- Kiosidou ED, Liarokapis DE, Tzabiras GD, Pantelis DI. 2017. Experimental investigation of roughness effect on ship resistance using flat plate and model towing tests. *J Ship Res.* 61:75–90.
- Larsson AI, Mattsson-Thorgren L, Granhag LM, Berglin M. 2010. Fouling-release of barnacles from a boat hull with comparison to laboratory data of attachment strength. *J Exp Mar Biol Ecol.* 392:107–114.
- Lewkowicz A, Das D. 1986. Turbulent boundary layers on rough surfaces with and without a pliable overlayer: a simulation of marine fouling. *Int Shipbuild Prog.* 33:174–186.
- Loeb G, Laster D, Gracik T. 1984. The influence of microbial fouling films on hydrodynamic drag of rotating discs. In: Costlow JD, Tipper R, editors. *Marine biodeterioration: an interdisciplinary study*. Annapolis (MD): Naval Institute Press; p. 88–94.
- Macdonald RW. 2000. Modelling the mean velocity profile in the urban canopy layer. *Bound-Layer Meteor.* 97:25–45.
- McEntee W. 1915. Variation of frictional resistance of ships with condition of wetted surface. *Trans Soc Nav Arch Mar Eng.* 24:37–42.
- Mizzi K, Demirel YK, Banks C, Turan O, Kaklis P, Atlar M. 2017. Design optimisation of propeller boss cap fins for enhanced propeller performance. *Appl Ocean Res.* 62:210–222.
- MontyJP, Dogan E, Hanson R, Scardino AJ, Ganapathisubramani B, Hutchins N. 2016. An assessment of the ship drag penalty arising from light calcareous tubeworm fouling. *Biofouling.* 32:451–464.
- Newman WA, Abbott DP. 1980. Cirripedia: the barnacles. In: Morris RH, Abbott DP, Haderlie EC, editors. *Intertidal invertebrates of California*. Stanford: California Stanford University Press; p. 504–535. Available from: <https://research.nhm.org/publications/page.html>
- Nikuradse J. 1933. Laws of flow in rough pipes. NACA Technical Memorandum 1292.
- Schoenherr KE. 1932. Resistances of flat surfaces moving through a fluid. *Trans SNAME.* 40:279–313.
- Schultz MP. 1998. The effect of biofilms on turbulent boundary layer structure [PhD thesis]. Melbourne (FL): Florida Institute of Technology.
- Schultz MP. 2000. Turbulent boundary layers on surfaces covered with filamentous algae. *J Fluids Eng.* 122:357–363.
- Schultz MP. 2004. Frictional resistance of antifouling coating systems. *J Fluids Eng.* 126:1039–1047.
- Schultz MP. 2007. Effects of coating roughness and biofouling on ship resistance and powering. *Biofouling.* 23:331–341.
- Schultz MP, Bendick JA, Holm ER, Hertel WM. 2011. Economic impact of biofouling on a naval surface ship. *Biofouling.* 27:87–98.
- Schultz MP, Flack K. 2007. The rough-wall turbulent boundary layer from the hydraulically smooth to the fully rough regime. *J Fluid Mech.* 580:381–405.
- Schultz MP, Swain G. 1999. The effect of biofilms on turbulent boundary layers. *J Fluids Eng.* 121:44–51.
- Schultz MP, Swain GW. 2000. The influence of biofilms on skin friction drag. *Biofouling.* 15:129–139.
- Swain GW, Kovach B, Touzot A, Casse F, Kavanagh CJ. 2007. Measuring the performance of today's antifouling coatings. *J Ship Prod.* 23:164–170.
- Tezdogan T, Demirel YK, Kellett P, Khorasanchi M, Incecik A, Turan O. 2015. Full-scale unsteady RANS CFD simulations of ship behaviour and performance in head seas due to slow steaming. *Ocean Eng.* 97:186–206.

- Turan O, Demirel YK, Day S, Tezdogan T. 2016. Experimental determination of added hydrodynamic resistance caused by marine biofouling on ships. *Transp Res Proc.* 14:1649–1658.
- Walker JM, Schultz MP, Flack KA, Steppe CN. 2014. Skin-friction drag measurements on ship hull coating systems. *Proceedings of the Thirtieth Symposium on Naval Hydrodynamics*; Nov 2–7; Hobart, Tasmania. p. 1–10. ISBN 978-1-86295-850-0. Available from: <http://ecite.utas.edu.au/96779>
- Watanabe S, Nagamatsu N, Yokoo K, Kawakami Y. 1969. The augmentation in frictional resistance due to slime. *J Kansai Soc Nav Arc.* 131:45–53.
- Woods Hole Oceanographic Institution. 1952. *Marine fouling and its prevention.* Annapolis (MD): United States Naval Institute.